Nat Hazards (2018) 90:803–822
https://doi.org/10.1007/s11069-017-3072-3

ORIGINAL PAPER

Seismic vulnerability of air traffic control towers

Mohammadreza Vafaei[1] · **Sophia C. Alih**[2]

Received: 23 January 2017 / Accepted: 21 October 2017 / Published online: 31 October 2017

Abstract Airports are one of the critical infrastructures that play an essential role in managing natural disasters through receiving or sending aid and supplies. Air traffic control (ATC) towers are an inseparable part of each airport as the performance of airports depends on the functionality of their ATC towers. Many ATC towers have been designed and constructed based on older versions of modern seismic codes in which seismic design has followed a force-based design approach. This study addresses the seismic vulnerability of three in-service ATC towers which have been designed and constructed according to a force-based design concept. The height of the towers ranges from 24 to 52 m. Fragility curves have been used for the seismic vulnerability study of these towers. For the derivation of seismic fragility curves, 45 earthquake records were selected and classified into low, medium and high classes based on their ratio of peak ground acceleration (PGA) to peak ground velocity (PGV). It was observed that records with a low PGA/PGV ratio imposed the highest level of damage to the towers. However, when towers were subjected to the records with a high PGA/PGV ratio, the damage intensity was not significant. Results indicated that the intensity of seismic-induced damage to the tallest tower was significantly more than that of the shortest tower. It was concluded that only the shortest tower could satisfy the expected seismic performance objectives.

Keywords ATC tower · Fragility curves · Incremental dynamic analysis · Concrete wall · Seismic damage

✉ Mohammadreza Vafaei
vafaei@utm.my

Sophia C. Alih
sophiacalih@utm.my

[1] Center for Forensic Engineering, Faculty of Civil Engineering, Universiti Teknologi Malaysia, 81310 Skudai, Johor, Malaysia

[2] Institute of Noise and Vibration, Faculty of Civil Engineering, Universiti Teknologi Malaysia, 81310 Skudai, Johor, Malaysia

1 Introduction

The occurrence of severe earthquakes adjacent to highly populated cities during past decades has caused disaster mitigation authorities and insurance companies to show more attention towards the seismic risk assessment of structures. Observations from past earthquakes have helped researchers to drive a statistical correlation between structural damages and the intensity of ground motions in the form of fragility curves (Charvet et al. 2014; De Luca et al. 2014). Fragility curves describe the conditional probability of various damage levels due to earthquake scenarios and have become one of the necessary tools for earthquake loss estimation and seismic risk analysis (Calvi et al. 2006; Elnashai and Di Sarno 2015). They also enable rapid structural assessment after an earthquake and have been used to determine the effectiveness of different seismic rehabilitation methods (Siqueira et al. 2014). Derivation of fragility curves from the observed seismic-induced damages is considered to be the most reliable approach as it truly incorporates all damage-related parameters (Mwafy 2012). However, the empirical approach loses its efficiency and feasibility when there are no informative damage observations for different site conditions or structural systems. Experimental tests have been performed for the derivation of fragility curves where not enough real data have been collected from site investigations (Siqueira et al. 2014; Cosenza et al. 2015). However, experimental tests for the derivation of fragility curves are often costly and time-consuming. Analytical approaches have been introduced as an alternative to that of observational and experimental methods (Ji et al. 2007; Kwon and Elnashai 2006). In the analytical methods, the required damage data are generated through extensive analytical simulations considering seismic hazard scenarios and structural systems. The rapid increase in the power of computers for performing structural analysis has made the analytically derived fragility curves the most realistic and cost-effective option (Mwafy 2012). It is worth mentioning that some researchers have also combined empirical and analytical approaches to reduce computational effort, cover for the lack of damage data and calibrate analytical models (Barbat et al. 1996; Kappos et al. 1998). More effective techniques have also been proposed to enhance derivation of analytically obtained fragility curves and reduce their extensive analytical simulations (Paolacci and Giannini 2009; Saha et al. 2013). Several researchers have employed analytical methods to drive seismic fragility curves of a specific group of structures including bridges (Siqueira et al. 2014; Bhatnagar and Banerjee 2015), tunnels (Argyroudis and Pitilakis 2012), non-ductile reinforced concrete frames (Celik and Ellingwood 2010; Rajeev and Tesfamariam 2012), steel braced frames (Lignos and Karamanci 2013), steel tanks (Buratti and Tavano 2014; Paolacci et al. 2015), reinforced concrete chimneys (Zhou et al. 2015), reinforced concrete buildings (Bilgin 2013; Hsieh et al. 2013; Modica and Stafford 2014; Sarno et al. 2013), masonry structures (Negulescu et al. 2014), wind turbine (Kim et al. 2014; Quilligan et al. 2012), high voltage disconnect switches (Paolacci et al. 2014) and process towers (Moharrami and Amini 2014).

ATC towers are one of the vital infrastructures in each airport because they control taking off and landing of aeroplanes. However, the seismic performance of existing ATC towers has not been reported during past earthquakes. This is because the number of existing ATC towers is limited in comparison with building structures. Furthermore, not all the existing ATC towers have been constructed in seismic prone areas. Therefore, unlike building structures, it has been difficult to investigate their real seismic behaviour during past earthquakes (Vafaei and Alih 2017). A review of the literature also shows that despite the significant role that ATC towers play in the mitigation of seismic-induced disasters,

only a few studies have addressed their seismic vulnerability (Vafaei et al. 2013; Moravej et al. 2016; Wilcoski and Heymsfield 2002). However, these studies have not been involved in a probabilistic evaluation approach and have focused only on a specific type of ATC towers. It is also noteworthy that seismic design codes have paid less attention to the seismic design and performance of ATC towers. Taking into account the importance of these structures, the variety in their lateral load resisting system, and the limited amount of published literature on this subject, more research is needed to better understand their seismic design and performance.

The main aim of the current study is to assess the seismic vulnerability of ATC towers that have been designed based on the force-based concept through a probabilistic framework. What makes this study important is that many existing ATC towers that have been constructed decades ago were not designed based on modern approaches like performance-based design method. Therefore, it would be of great interest to investigate their vulnerability against earthquakes and if needed decide on their retrofit strategies.

In this study, three in-service ATC towers with different heights but similar structural systems have been selected for seismic fragility assessment. The seismic design of these towers is based on the Iranian Code of Practice for Seismic Resistant Design of Buildings (ICPSRD 2005). In the next section, the selected towers are presented in detail. The employed methodology for the derivation of fragility curves and discussion on the obtained results are explained in the subsequent sections.

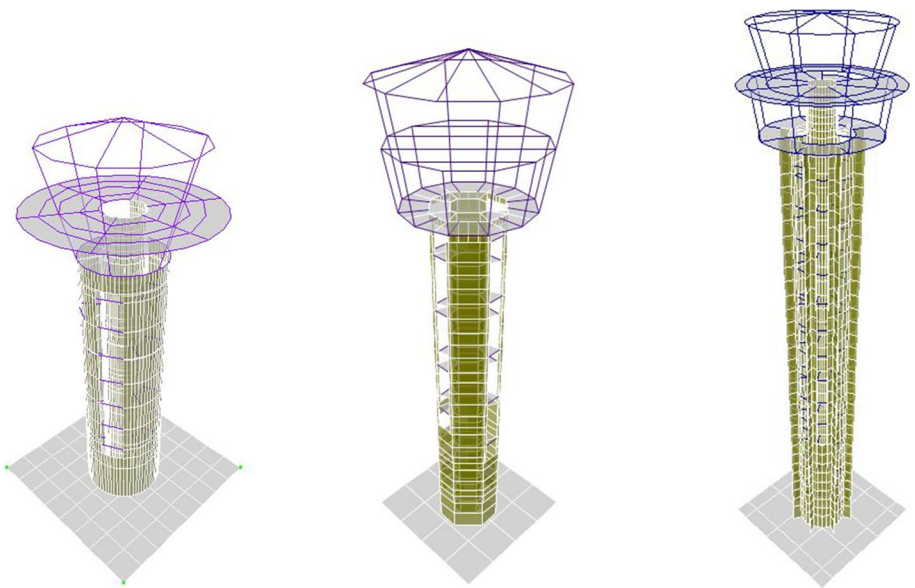

Fig. 1 Selected ATC towers. **a** Tower 1, **b** Tower 2, **c** Tower 3

2 Selected towers

This section provides details regarding the towers that have been studied in this paper. Figure 1 shows the finite element (FE) model of the selected ATC towers. As can be seen from this figure, along the height, all towers are composed of two different structural systems. At the top, where equipment and observation rooms are located, towers are equipped with the steel moment-resisting frame (MRF). The top structure sits on two concrete cores that transfer actions from MRF to the foundation. The concrete cores settle on a mat foundation with the thickness of 120, 130, and 150 cm for Tower 1 to Tower 3, respectively. The towers are protected against overturning through the weight and the size of their foundation. The concrete cores have different cross sections. However, along the height, the thicknesses of concrete cores are constant as shown in Fig. 2. The longitudinal reinforcement ratios of concrete cores vary from 0.68 to 1.3% for interior concrete cores and from 0.42 to 1.7% for exterior concrete core. Staircases are placed between interior and exterior concrete cores, and lifts are positioned inside the interior concrete cores. Columns of MRFs have a box-shaped cross section and all are tilted 25 degrees out of vertical axis. The size of tilted columns is identical for each tower; however, the cross-sectional size varies from one tower to another. The sizes of columns for Tower 1 to Tower 3 are 25×25 cm, 30×30 cm, and 30×20 cm, respectively. All beams have an I-shaped cross section and are fully welded to the columns. The height of beams varies from 30 to 35 cm while their flange width is 20 cm. The steel used for the construction of beams and columns has the yield stress of 240 MPa, ultimate tensile strength of 370 MPa and the elastic modulus of 200 GPa. The steel columns of superstructures in Tower 2 and Tower 3 sit on a concrete slab with the thickness of 40 cm using steel base plates with the thickness of 3 cm. In Tower 1, the steel columns of the superstructure are directly connected to the outer concrete core through base plates with the thickness of 3 cm. All base plates have eight steel bolts with a diameter of 2.8 cm. The steel columns are fully welded to their base plates through eight stiffeners with the thickness of 1.5 cm resulting in a rigid connection. More details regarding the selected towers are presented elsewhere (Vafaei and Alih 2016).

Seismic design of towers follows the recommendations of Iranian Code of Practice for Seismic Resistant Design of Buildings (ICPSRD 2005). ICPSRD employs the force-based design concept and has no specific constraints on the allowable drift for non-building structures like ATC towers unless disregarding the drift can lead to fatality. According to

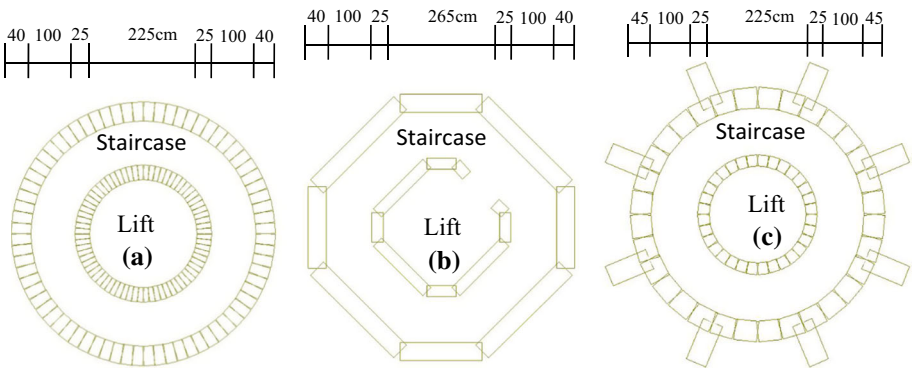

Fig. 2 Cross sections of the ATC towers. **a** Tower 1, **b** Tower 2, **c** Tower 3

ICPSRD, seismic analysis of non-building structures with the fundamental natural period of 0.5 and more should be based on a dynamic analysis (response spectrum or time history analysis). For these types of structures, equivalent static analysis can be only employed to estimate their design base shear. Table 1 displays design base shears and design natural periods of the selected towers that have been calculated based on ICPSRD. The design periods that are obtained from finite element models are based on un-cracked section properties and represent the natural period of the first mode of vibration. The effective modal mass of the first mode shape for Tower 1, Tower 2 and Tower 3 are 68, 66, and 57%, respectively. Moreover, in the dynamic analysis, consideration of the first 12 mode shapes of the towers ensured the cumulative effective modal mass of more than 90%.

It should be mentioned that the design peak ground acceleration (PGA) for all towers was 0.3 g and that all towers have been constructed on site class D of ASCE/SEI 7-10 (2010) (i.e., 175 m/s $<$ shear wave velocity $<$ 375 m/s). Figure 3 displays the 5% damped design response spectrum that has been employed for the seismic design of towers. For the derivation of seismic fragility curves, incremental dynamic analysis (IDA) was used (Vamvatsikos and Cornell 2002, 2004). FE models of the towers were established using PERFORM-3D (Computers and Structures, CSI 2006) software considering all details given in their structural drawings. This software has been widely employed by researchers for inelastic analysis of structures (Reyes and Chopra 2011; Epackachi et al. 2012; Yang et al. 2012; Berahman 2013), and its capability in simulating the nonlinear behaviour of concrete walls has been verified by experimental studies (Schotanus and Maffei 2008; Jiang and Liu 2011). A review of the literature shows that the modelling methods of concrete walls can be categorized into four distinct groups that include fibre element models, lumped plasticity models, macro-models and continuum finite element models. Each of these modelling approaches has its advantages and disadvantages. For instance, the lumped plasticity models offer a simple and computationally efficient approach which allows an analyst to account for tension stiffening effects and the shape of hysteresis loops (Wilson 2003). However, they need extensive calibration with experimental results and can only predict the overall response of concrete walls (i.e., unable to display the cracking of concrete walls and strain distribution in their reinforcements). In comparison, fibre element and macro-models can provide an accurate estimation of stiffness degradation, energy dissipation and lateral load responses (Jiang and Kurama 2010; Orakcal and Wallace 2006). However, these models for structures that show limited flexural cracking and localization of strains before failure (e.g., lightly reinforced concrete walls) may not lead to accurate results (Lu and Henry 2017). The most detailed global and local response of RC walls can be captured by continuum finite element model, but they require accurate multiaxial constitutive material models and are computationally time-consuming. Considering the advantages and disadvantages of the above-mentioned models, the fibre

Table 1 Design base shears and natural periods of towers

ATC towers	Total height (m)	Total design weight (MN)	Design base shear (kN)	Design periods (Sec.)
Tower 1	23.7	4.20	980.4	0.44
Tower 2	39.3	8.89	1867.8	1.05
Tower 3	51.7	15.02	3154.7	1.81

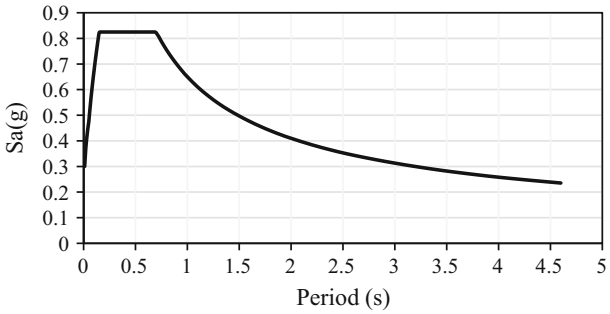

Fig. 3 5% damped response spectrum used for the design of towers

element model was selected because it has the efficiency of a simplified model and the refinements of a microscopic model (Lu and Henry 2017).

PERFORM-3D employs the inelastic fibre elements to simulate the inelastic behaviour of concrete walls. As can be seen from Fig. 4, the combined behaviour of three main layers defines the behaviour of fibre elements. The layers interact and they are connected to similar nodes. These three layers are (a) an inelastic axial-bending fibre section that acts as vertical reinforcements and gross concrete area, (b) an axial-bending fibre section for the horizontal axis that has a linear cross section for reinforcements and concrete, and (c) a conventional shear layer with a uniform wall thickness. In addition to the main three layers, PERFORM-3D also allows for two more diagonal layers to account for the contribution of reinforcing steel to the shear strength. The diagonal layers should only be included in the analysis when the diagonal strut action is important. Considering the cylindrical shape of concrete walls in the ATC towers, their flexural behaviour and the low shear stress obtained in concrete walls, the effect of diagonal layers was ignored in the modelling of ATC towers and only the conventional shear layer (see Fig. 4c) was employed. It is worth noting that the strut and tie behaviour is complex and a model that includes this behaviour may over-estimate the shear strength of a wall (CSI 2006). Moreover, FEMA 356 (2000) considers only the conventional shear layer and ignores the strut and tie action in the seismic behaviour of concrete walls. The out-of-plane bending of concrete walls is modelled elastic due to its insignificant effect on the behaviour of concrete walls. The hysteretic

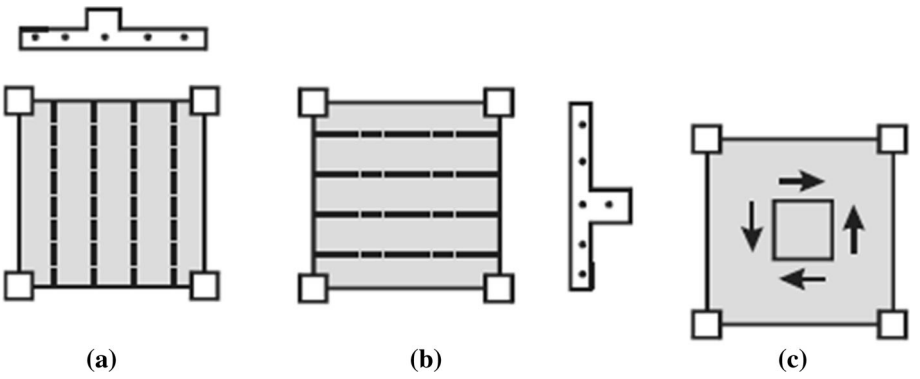

Fig. 4 Parallel layers used in PERFORM-3D for modelling of concrete walls (CSI 2006). **a** Vertical axial/bending, **b** horizontal axial/bending, **c** concrete shear

behaviour of fibre elements in the axial-bending layer follows a tri-linear model that can have in-cycle strength deterioration and cycle stiffness degradation (CSI 2006).

Nonlinear behaviour of beams and columns was simulated by using lumped plastic hinges assigned to the end of each member. Figure 5 displays the typical force–deformation relationship of a plastic hinge that can be defined in PERFORM-3D. In this figure, segment AB indicates the elastic behaviour, segment BC represents the post-yield behaviour and segment CD shows the beginning of the failure. The parameters for each member in the figure were extracted from the tables provided in FEMA 356 (2000) considering material properties, internal forces and sizes of beams and columns. It should be mentioned that the three-dimensional axial force-bending moment interaction diagrams were used to calculate column capacities.

For the elastic range, the software can consider viscous damping through Modal and Rayleigh damping. In the present study, mass and stiffness proportional parameters of the Rayleigh damping were selected such that the mode shapes with the frequency equal to the first mode and 20% of the first mode have 3% viscous damping. This resulted in damping ratios ranging from 2.4 to 8.7% for the first 12 vibration modes of the ATC towers. It is important to mention that just like concrete chimneys (Zhou et al. 2015) ATC towers have low damping especially when compared with building structures. This is mainly due to this fact that in ATC towers, some sources of energy dissipation like partitions, ceilings and other non-structural components are less than that of other building structures. Therefore, following the previous studies (Zhou et al. 2015; Muthukumar and Sabelli 2013), this study employs a lower damping ratio (i.e., 3%) than that of usual practice for concrete structures (i.e., 5%). For the inelastic range, the hysteretic damping of concrete walls was simulated through the material hysteresis models. In PERFORM-3D, for a concrete fibre, the unloading stiffness is always equal to the initial elastic stiffness and the dissipated energy is controlled by changing the reloading stiffness. In this study, for concrete material, the degradation rule of Mander model for unloading and reloading stiffnesses is used.

Figure 6 displays the employed stress–strain relationships for concrete and reinforcement fibres. It is worth mentioning that usually the expected material strength, which can be larger than nominal strength, is used for the nonlinear analysis. However, in this study, the nominal strength of the material is used. Winkler's spring model was employed to simulate soil behaviour beneath the foundations. The stiffness of springs was calculated using geotechnical properties obtained from on-site soil investigations. Compressive

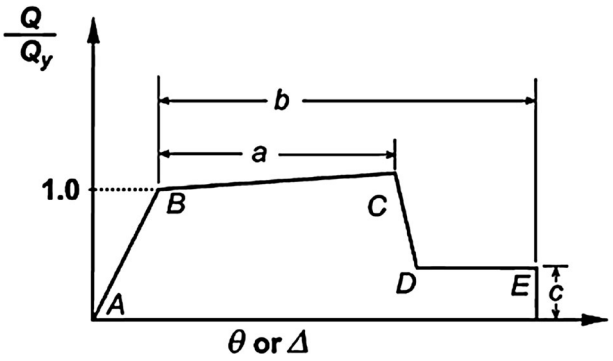

Fig. 5 Generalized chord rotation model used for inelastic behaviour of beams and columns (FEMA 356 2000)

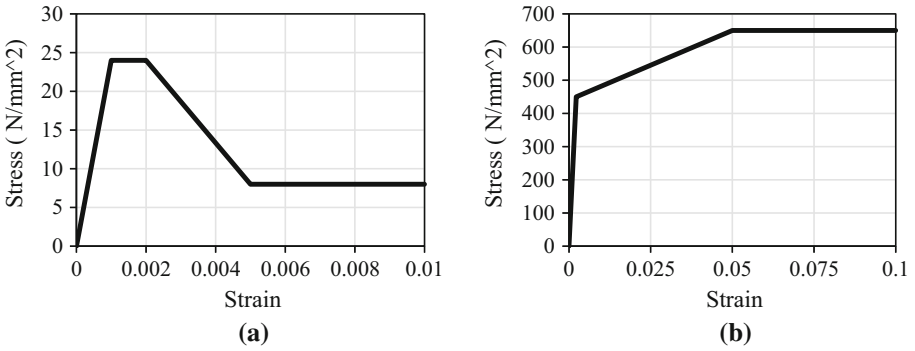

Fig. 6 Stress–strain relationships used for **a** concrete and **b** reinforcements

stiffness of soil was only included in the analysis. The mat foundations of ATC towers were simulated using the General Wall element provided in PERFORM-3D software. Following the recommendation of FEMA 356 (2000), an equivalent elastic–plastic model was considered for foundation load-deformation characteristics and it was simulated in the software by using the inelastic bar element (CSI 2006). Moreover, each spring's vertical stiffness property was calculated by dividing the total vertical stiffness of the foundation to the corresponding area of the spring. The rotational stiffness properties were calculated by dividing the total rotational stiffness of the footing by the moment of inertia of the footing in the direction of loading (FEMA 356 2000). In the analysis, vertical and rotational stiffness were decoupled using the procedure recommended in FEMA 356 (2000). The P-delta effect was also included in all analysis.

3 Consideration of uncertainties

There are two types of uncertainties that contribute to the seismic fragility assessment of structures: those which are inherently random (aleatoric) and those that are due to the lack of knowledge (epistemic) (Wen et al. 2004). Since it is not practical to consider all uncertain parameters for the fragility assessment of structures, it is crucial to identify the most influential parameters. Extensive research has revealed that compared to variability in ground motions, uncertainties in material properties have little impact on the seismic fragility of structures (Kwon and Elnashai 2006; Kinali and Ellingwood 2007; Porter et al. 2002). The study by Celik and Ellingwood (2010) on the non-ductile reinforced concrete frames also confirmed that uncertainties in material and structural parameters like structural damping, concrete strength, and cracking strain in beam–column joints have less impact on the obtained seismic fragilities when compared to uncertainties in seismic demands from earthquakes. Considering the findings above, variability in the ground motion intensities was only included in the derivation of seismic fragilities. Material properties were considered deterministic and were set equal to their mean values.

To account for uncertainty in seismic demands, 45 natural earthquake records classified into three specific groups (each containing 15 records) were selected. Classification of the groups was determined based on the PGA/PGV ratio of the records. Tso et al. (1992) showed that PGA/PGV ratio is a simple parameter that can indicate the relative frequency content and duration of earthquake ground motions generated by different seismic

environments. Ground motion PGA/PGV ratio also has a significant effect on the peak inelastic response, hysteretic energy dissipation and stiffness deterioration of stiffness degrading systems (Zhu et al. 1988). Following similar classification to that of TSO et al., herein, earthquake records with the PGA/PGV < 0.8 g/m/s, $0.8 \leq$ PGA/PGV ≤ 1.2 and PGA/PGV > 1.2 were grouped as low, medium and high range, respectively, and they have been referred to as low-class, medium-class and high-class records. Such classification allowed for further study about the effect of PGA/PGV ratio of records on the seismic fragility of the selected towers. Figures 7 and 8 display the magnitude and PGA/PGV ratio of selected earthquake records against their source distances, respectively. It can be seen that high PGA/PGV ratio characterizes motions in the vicinity of earthquake sources while low PGA/PGV ratio displays motions far from large earthquakes (Tso et al. 1992).

4 Derivation of fragility curves

Fragility curves show the conditional probability of various damage levels due to earthquake scenarios. In the present study, seismic fragility curves were obtained using Eq. (1) (Wen et al. 2004):

$$\mathrm{P(DS|SI)} = 1 - \Phi\left(\frac{\lambda_{\mathrm{C}} - \lambda_{\mathrm{D|SI}}}{\sqrt{\beta_{\mathrm{D|SI}}^2 + \beta_{\mathrm{C}}^2 + \beta_{\mathrm{M}}^2}}\right) \tag{1}$$

$$\beta_{\mathrm{D|SI}} = \sqrt{\ln(1 + S^2)} \tag{2}$$

where P(DS|SI) is the conditional probability of exceeding a damage state (DS) for a given seismic intensity (SI). Φ is the standard normal distribution; λ_{C} is the natural logarithm of the median of the drift capacity for a particular damage state; $\lambda_{\mathrm{D|SI}}$ is the natural logarithm of calculated median demand drifts given the seismic intensity from the best fit power law line. S^2 is the standard error and ln is the natural logarithm. $\beta_{\mathrm{D|SI}}$ stands for demand uncertainty while β_{c} and β_{M} reflect uncertainties associated with capacity and modelling, respectively. In this study, β_{M} were assumed to be 0.3 as done in existing literature (Wen

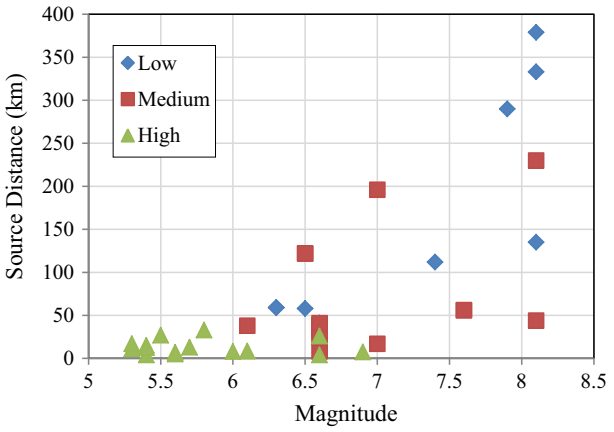

Fig. 7 Magnitude of the selected records against their source distances

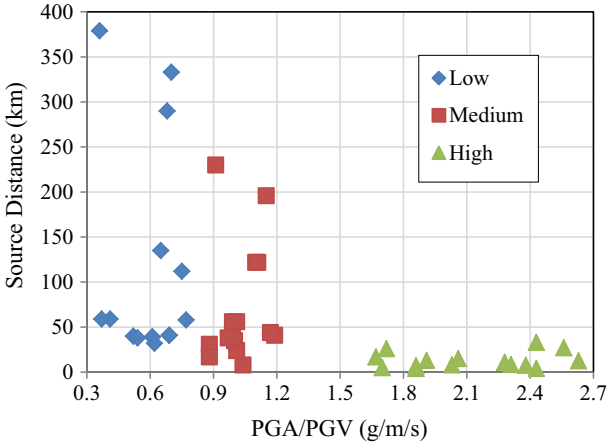

Fig. 8 PGA/PGV ratios of the selected records against their source distances

et al. 2004; Mwafy 2012). The value of β_c was taken as $\sqrt{\ln(1 + \text{Cov.}^2)}$(Wen et al. 2004) and was separately calculated for each limit state capacities and each class of earthquake records using the results obtained from IDA. In this equation, Cov. is the coefficient of variation of the calculated limit state capacities. Table 2 displays the calculated values for β_c.

Precise determination of drift capacities at the specified damage states is crucial when deriving seismic fragility curves. Three structural damage states have been introduced in FEMA 356 (2000) including immediate occupancy (IO), life safety (LS) and collapse prevention (CP). The IO damage state indicates that structures can be occupied immediately after earthquakes with little or no repair. Damage to structures in the LS performance level is significant; however, structures provide a reasonable safety margin against collapse. The CP damage state structures continue to support gravity loads but retain no margin against collapse. For different structural systems, drift capacities for the damage states have been presented in the code. For instance, FEMA 356 (2000) recommends 0.5% of transient or negligible permanent drift for IO performance level, 0.5% permanent or 1% transient drift for LS performance level and 2% permanent or transient drift for CP performance level. Negligible, minor to moderate, moderate to major and collapse are four damage states that have been recommended by the SEAOC Blue Book (1999) for concrete wall structures, and drift capacities ranging from 0.4 to 2.1% have been considered for

Table 2 Calculated drift capacity uncertainties associated with the limit states for each tower

Class of record	Limit state	Tower 1	Tower 2	Tower 3
Low	IO	0.09	0.22	0.21
	LS	0.09	0.17	0.19
	CP	0.12	0.14	0.16
Medium	IO	0.06	0.21	0.2
	LS	0.1	0.22	0.18
	CP	0.11	0.18	0.2
High	IO	0.11	0.27	0.21
	LS	0.10	0.27	0.23
	CP	0.13	0.21	0.24

them. Similar to FEMA 356 (2000), ASCE/SEI 41-06 (2006) has introduced three levels of damage intensity for concrete wall structures that include immediate occupancy, life safety and collapse prevention. ASCE/SEI 41-06 (2006) recommends 0.5, 1 and 2% of inter-story drift ratios (IDRs) as limit states for IO, LS and CP drift capacities, respectively. In addition to the building codes, IDR has been widely accepted by researchers as a global damage indicator (Rajeev and Tesfamariam 2012; Ghobarah 2004; Kircher et al. 1997). While the code recommended IDRs include a safety margin, the proposed IDRs by researchers are often less conservative. Kircher et al. (1997), for low-rise concrete shear wall buildings designed in accordance with UBC97 (Uniform Building Code 1997) requirements, recommended IDRs of 2.3 and 6% for extensive and complete damage states, respectively. Rajeev and Tesfamariam (2012), for non-ductile moment resistance concrete frame, employed IDRs of 1, 2 and 4% for IO, LS, and CP limit states, respectively. The discrepancy in the recommended IDRs implies that, for a precise analysis, drift capacities corresponding to damage states should be defined separately for each structure.

Following the recommendation of FEMA 356 (2000), in the present study, three damage states which are termed as immediate occupancy, life safety and collapse prevention were considered. To calculate drift capacity of towers at the specified damage states, acceptance criteria for beams, columns and concrete shear walls were determined. In the present study, the acceptance criteria for beams and columns at each damage state followed the threshold given by FEMA 356 (2000). For concrete walls, the thresholds of damage states were defined in accordance with the strain levels in concrete and reinforcements. Table 3 displays the considered thresholds for IO, LS and CP damage states. It is worth noting that the considered CP thresholds for concrete and reinforcements are in accordance with the recommendations of FEMA 356 (2000). The selected thresholds are also comparable with the selected values by other researchers (Zhou et al. 2015; Priestley 1997).

For each damage state, drift capacities of towers were calculated through extensive incremental dynamic analysis, considering the acceptance criteria defined for beams, columns and concrete shear walls. In some studies, drift capacities have been calculated through pushover analysis by tracing the sequence of yielding and failure of structures (Mwafy 2012; Shinozuka et al. 2000). However, since some studies have shown that the application of pushover analysis for ATC towers may not lead to accurate results (Vafaei et al. 2013), herein, the incremental dynamic analysis is employed. Tables 4 and 5 display the minimum and median drift capacities obtained for each tower and each class of earthquake record. It is important to note that for the calculation of drift values, at first, the shafts of towers were divided into small segments considering the level of stair landings that are located between the inner and outer concrete cores (see Fig. 2). This led to segments with almost identical heights of 3.2 m. The difference of the deflections at the centres of mass at the top and bottom of each segment was considered as the storey drift for

Table 3 Considered strain thresholds in concrete and reinforcements

Damage state	Strain in concrete	Strain in reinforcement
IO	0.002	0.01
LS	0.003	0.025
CP	0.005	0.05

Table 4 Minimum of drift capacities obtained from IDA

Record class	Tower 1			Tower 2			Tower 3		
	IO (%)	LS (%)	CP (%)	IO (%)	LS (%)	CP (%)	IO (%)	LS (%)	CP (%)
Low	2.1	3.18	3.87	1.32	2.3	3.08	1.04	1.48	2.04
Medium	2.2	3.07	3.73	0.92	1.8	2.60	0.94	1.63	2.00
High	1.96	2.69	3.3	0.93	1.54	2.10	1.13	2.01	2.69

Table 5 Median of drift capacities obtained from IDA

Record class	Tower 1			Tower 2			Tower 3		
	IO (%)	LS (%)	CP (%)	IO (%)	LS (%)	CP (%)	IO (%)	LS (%)	CP (%)
Low	2.80	3.75	4.65	1.57	3.50	4.30	1.37	1.93	2.66
Medium	2.60	3.85	4.63	1.46	2.78	3.40	1.57	2.40	2.96
High	2.50	3.37	4.18	1.10	2.80	3.1	1.70	2.82	3.64

that segment. The storey drifts obtained from concrete cores together with those obtained from observation and equipment levels were included in the calculation of fragility curves.

It is evident from the median of drift capacities (see Table 5) that the ATC towers show considerably higher drift capacities compared to the recommended values by building codes especially for the IO damage state. The reason for such higher drift capacities relies on the fact that in the studied ATC towers, the maximum IDRs occurred at the observation room level, where towers faced a sudden significant decrease in the lateral stiffness due to the absence of concrete shear walls. While this observation is in line with the findings of other researchers (Moravej et al. 2016; Wilcoski and Heymsfield 2002), structural damage mostly formed at the lower levels of concrete walls. This is because the axial forces in the columns of the observation rooms were very low (due to the usage of light weight roofs), so the columns could tolerate a higher level of IDRs before reaching the thresholds of the acceptance criteria. On the other hand, although the IDRs at the lower levels of concrete walls were significantly less than that of observation rooms, due to strain accumulation (from gravity and earthquake loads), the damage is mostly concentrated there. The capacities of connections between steel columns and concrete slabs in the superstructures of Tower 2 and Tower 3 were carefully investigated against seismic demands to ensure that they could safely carry the forces transferred to them by the steel columns. Results indicated that the connections and the concrete slabs remained in the elastic range during the seismic events and, therefore, had no significant influence on the seismic fragility of the studied ATC towers. Similar results were obtained for the connections between the steel columns and concrete walls of Tower 1.

Considering this fact that if a building has to be occupied after earthquakes non-structural components also should not have significant damage, for all towers, the drift capacity corresponding to the IO damage state was limited to the IDR of 1% (Rajeev and Tesfamariam 2012; Erberik 2008; Applied Technology Council 1996). Drift capacities corresponding to LS and CP damage states were determined for each tower individually using the minimum drift capacities obtained for each class of records. Table 6 displays the employed drift capacities for each damage state. It should be mentioned that, by selecting

the minimum drift capacities as the reference for all records, the derived fragility curves for the medium and high class of records become conservative.

It is worth mentioning that obtained results for drift capacities demonstrate the importance of considering PGA/PGV ratio of earthquake records in the derivation of fragility curves. As can be seen from Table 5, for TOWER 3, the low-class earthquake records provide lower drift capacities compared to the high-class records. In contrast, TOWER 2 has lower drift capacities when it is excited by the high-class records. For TOWER 1, the three different classes of records result in almost similar median drift capacities.

The statistical distributions of IDRs against PGA were used to estimate the probability of exceeding each damage state at different ground intensity levels. Figures 9, 10 and 11 depict such statistical distributions for the records having high PGA/PGV ratio along with the calculated power law equations and the coefficient of distributions (R2). As can be seen from Figs. 9, 10 and 11, in this study, peak ground acceleration is employed as the ground motion intensity measures. PGA was selected as the ground motion intensity measure because it agrees with the approach adopted by many seismic design codes. In previous studies, in addition to the vast usage of PGA, other types of ground motion intensity measures have also been used. Spectral acceleration, spectral displacement and spectral velocity are among the other employed intensity measures (Celik and Ellingwood 2010; Bilgin 2013).

Figures 12, 12, 13, 14, 15, 16, 17, 18, 19 and 20 display the generated seismic fragility curves for TOWER 1, TOWER 2 and TOWER 3, considering the three different classes of earthquake records. Results show that the low-class record imposes the maximum level of damage to all towers while the high-class records do not have a significant effect on them. The reason lies in the fact that, the low-class records are rich of low predominant frequencies that can significantly excite the first vibration mode of the ATC towers. On the other hand, the high-class records signify mostly high predominant frequencies which have not been very influential in the seismic behaviour of the studied towers. Figures also indicate that at the design PGA, the intensity of seismic-induced damage to towers increases as the height of towers increases. The main reason for the observed trend is the significant reduction in the over-strength factor of the ATC towers as their height increases (Vafaei and Alih 2016). A comparison among the slope of fragility curves shows that, for the low-class records, the slope becomes steeper as the height of tower increases. It can also be seen that as the height increases, the probability of exceeding IO and CP limit states become closer to each other. It is worth mentioning that, ATC towers are often expected to comply with two different seismic performance objectives; (1) immediate occupancy for the design basis earthquake (DBE) and (2) life safety for the maximum considered earthquake (MCE) (Vafaei et al. 2013). The PGA at the construction site of the studied towers is 0.3 g for the DBE level and 0.45 g for the MCE level. It is evident from the obtained fragility curves that for the low-class records,

Table 6 Employed drift capacities for each damage state

Tower 1			Tower 2			Tower 3		
IO	LS	CP	IO	LS	CP	IO	LS	CP
1.00%	2.70%	3.30%	1.00%	1.50%	2.1%	1.00%	1.50%	2.00%

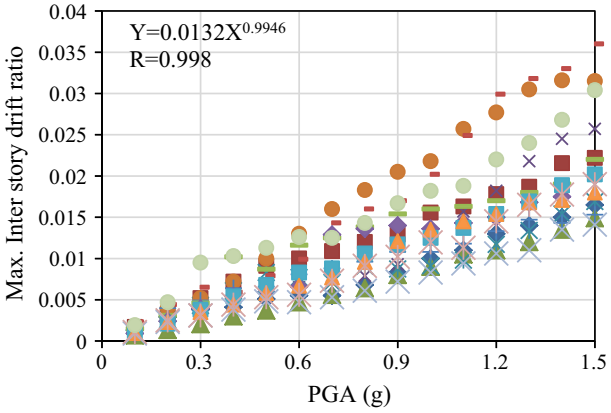

Fig. 9 Max. IDRs of TOWER 1 against different ground motion intensities

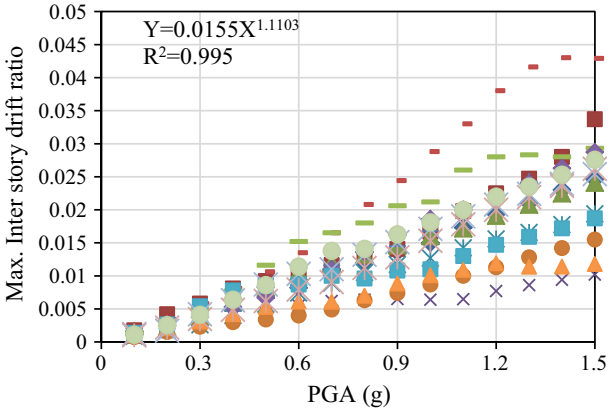

Fig. 10 Max. IDRs of TOWER 2 against different ground motion intensities

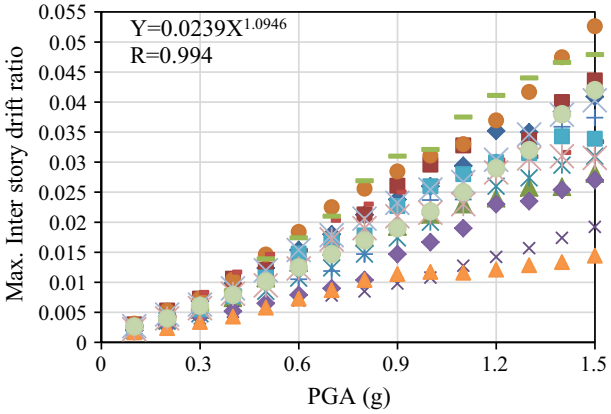

Fig. 11 Max. IDRs of TOWER 3 against different ground motion intensities

only TOWER 1 satisfies the aforementioned performance objectives. This shows the inadequacy of using the force-based design approach for the seismic design of the studied towers.

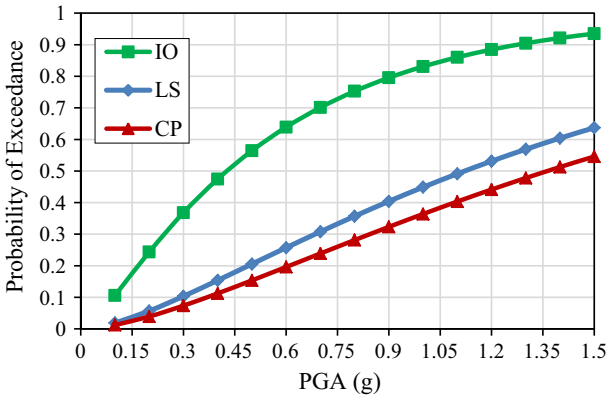

Fig. 12 Seismic fragility of Tower 1 considering the low class of PGA/PGV ratio

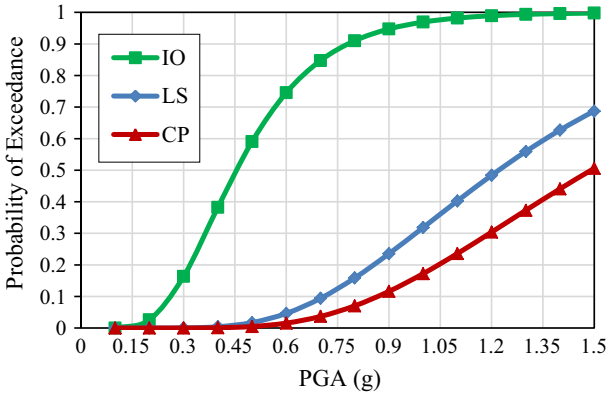

Fig. 13 Seismic fragility of Tower 1 considering the medium class of PGA/PGV ratios

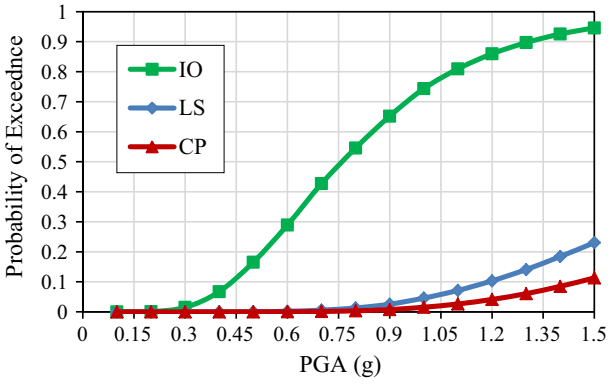

Fig. 14 Seismic fragility of Tower 1 considering the high class of PGA/PGV ratios

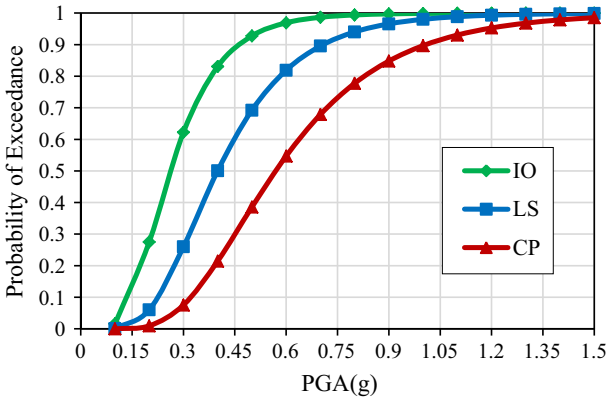

Fig. 15 Seismic fragility of Tower 2 considering the low class of PGA/PGV ratios

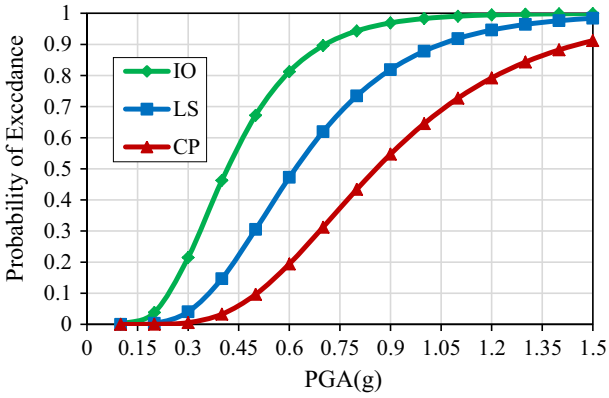

Fig. 16 Seismic fragility of Tower 2 considering the medium class of PGA/PGV ratios

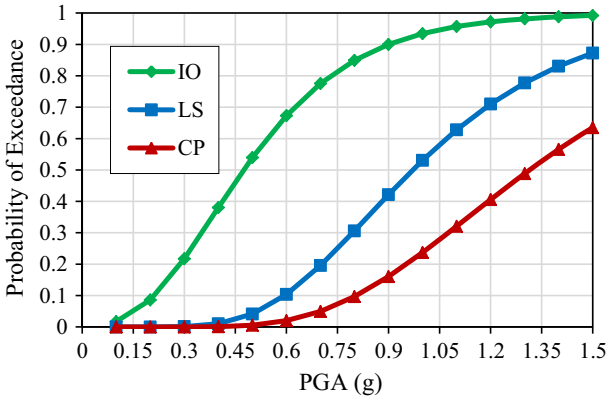

Fig. 17 Seismic fragility of Tower 2 considering the high class of PGA/PGV ratios

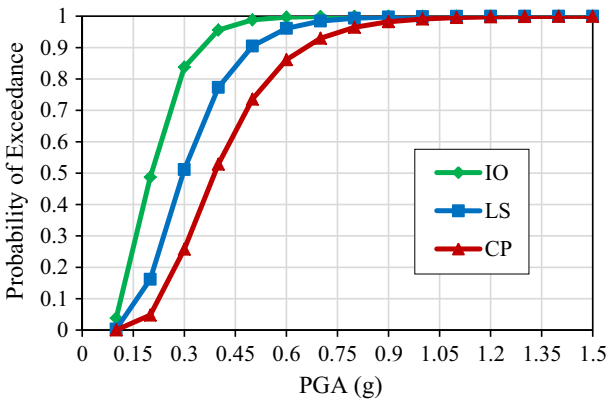

Fig. 18 Seismic fragility of Tower 3 considering the low class of PGA/PGV ratios

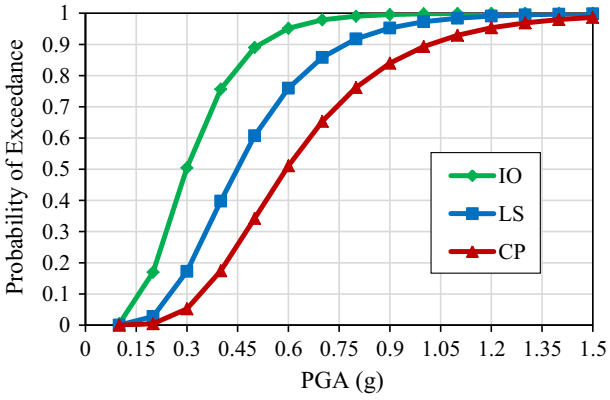

Fig. 19 Seismic fragility of Tower 3 considering the medium class of PGA/PGV ratios

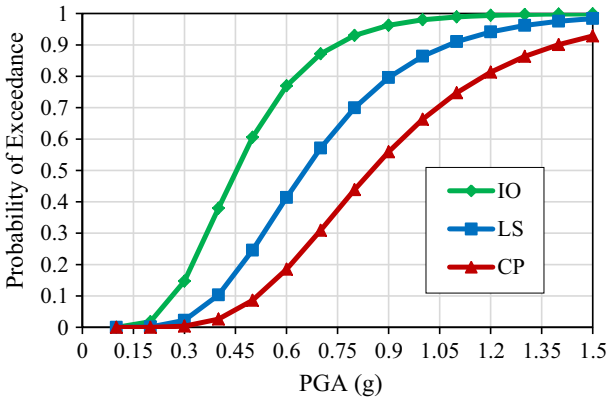

Fig. 20 Seismic fragility of Tower 3 considering the high class of PGA/PGV ratios

5 Conclusions

Air traffic control towers are vital infrastructures of which their seismic vulnerability has not been well researched. This study addressed the seismic fragility of three in-service ATC towers with the heights of 24, 39 and 52 m. The studied towers have been designed

and constructed according to a force-based design concept. The lateral load resisting system of the towers consisted of two concrete cores and a steel moment-resisting frame. The towers were subjected to 45 natural earthquake records which were classified into three main groups based on their PGA/PGV ratio. The fragility relationships of the reference ATC towers were obtained by relating the measured seismic responses from a large number of incremental dynamic analysis to the peak ground acceleration using a reliable statistical model. Results indicate that the tallest tower is significantly more vulnerable than the shortest tower. For a design PGA of 0.3 g and the low-class of records, the probability of exceeding IO, LS and CP levels for the 52 m-tall tower is 2.4, 5.4 and 3.2 times larger than that of the shortest tower, respectively. It was also observed that damage intensity was higher when towers were excited by records with lower PGA/PGV ratio. However, records with higher PGA/PGV ratio were less vulnerable for the studied towers. The probability of exceeding IO, LS and CP levels in the 52 m-tall tower for the low-class of records and the design PGA of 0.3 g are, respectively, 1.7, 1.9 and 7.3 times larger than those obtained for the high class of records and the same PGA. As the height of towers increased, the probability of exceeding IO and CP limit states got closer to each other, indicating smaller reserve strength in the towers. It can be concluded that the force-based design concept used for the seismic design of towers is only adequate in fulfilling the required performance objectives of the shortest tower.

Acknowledgements Authors would like to thank the constructive comments from anonymous reviewers. This study has been funded by the Ministry of Science, Technology and Innovation, Malaysia under the Grant No. R.J130000.7922.4S122 which is greatly appreciated. The support provided by Universiti Teknologi Malaysia is also acknowledged.

References

Applied Technology Council, ATC-40 (1996) Seismic evaluation and retrofit of concrete buildings, vols 1 and 2, California

Argyroudis SA, Pitilakis KD (2012) Seismic fragility curves of shallow tunnels in alluvial deposits. Soil Dyn Earthq Eng 35:1–12

ASCE/SEI 7-10 (2010) Minimum design loads for buildings and other structures. American Society of Civil Engineers, Reston

ASCE/SEI 41-06 (2006) Seismic rehabilitation of existing buildings, ASCE Standard. American Society of Civil Engineers, Reston

Barbat AH, Yépez Moya F, Canas JA (1996) Damage scenarios simulation for seismic risk assessment in urban zones. Earthq Spectra 12(3):371–394

Berahman F (2013) Performance-based seismic evaluation of the Icon Hotel in Dubai, United Arab Emirates. Struct Des Tall Spec Build 22(3):300–326

Bhatnagar UR, Banerjee S (2015) Fragility of skewed bridges under orthogonal seismic ground motions. Struct Infrastruct Eng 11(9):1113–1130

Bilgin H (2013) Fragility-based assessment of public buildings in Turkey. Eng Struct 56:1283–1294

Buratti N, Tavano M (2014) Dynamic buckling and seismic fragility of anchored steel tanks by the added mass method. Earthq Eng Struct Dyn 43(1):1–21

Calvi GM, Pinho R, Magenes G, Bommer JJ, Restrepo-Velez LF, Crowley H (2006) Development of seismic vulnerability assessment methodologies over the past 30 years. ISET J Earthq Technol 43(3):75–104

Celik OC, Ellingwood BR (2010) Seismic fragilities for non-ductile reinforced concrete frames—role of aleatoric and epistemic uncertainties. Struct Saf 32(1):1–12

Charvet I, Ioannou I, Rossetto T, Suppasri A, Imamura F (2014) Empirical fragility assessment of buildings affected by the 2011 Great East Japan tsunami using improved statistical models. Nat Hazards 73(2):951–973

Computers and Structures Inc. (CSI) (2006) PERFORM 3D. User guide v4, Non-linear analysis and performance assessment for 3D structures. Computers and Structures, Inc., Berkeley
Cosenza E, Di Sarno L, Maddaloni G, Magliulo G, Petrone C (2015) Shake table tests for the seismic fragility evaluation of hospital rooms. Earthq Eng Struct Dyn 44(1):23–40
De Luca F, Verderame GM, Manfredi G (2014) Analytical versus observational fragilities: the case of Pettino (L'Aquila) damage data database. Bull Earthq Eng 13(4):1161–1181
Elnashai AS, Di Sarno L (2015) Fundamentals of earthquake engineering, 2nd edn. Wiley, London
Epackachi S, Mirghaderi R, Esmaili O, Behbahani AAT, Vahdani S (2012) Seismic evaluation of a 56-storey residential reinforced concrete high-rise building based on nonlinear dynamic time-history analyses. Struct Des Tall Spec Struct 21(4):233–248
Erberik MA (2008) Generation of fragility curves for Turkish masonry buildings considering in-plane failure modes. Earthq Eng Struct Dyn 37(3):387–405
FEMA 356 (2000) Prestandard and commentary for the seismic rehabilitation of buildings. American Society of Civil Engineers, Reston
Ghobarah A (2004) On drift limits associated with different damage levels. In: Proceedings of 4th international workshop on performance-based seismic design, 28 June–1 July, Bled, Slovenia
Hsieh MH, Lee BJ, Lei TC, Lin JY (2013) Development of medium-and low-rise reinforced concrete building fragility curves based on Chi-Chi Earthquake data. Nat Hazards 69(1):695–728
Iranian Code of Practice for Seismic Resistant Design of Buildings (ICPSRD) (2005) Standard No. 2800, 3rd edn. Building Housing Research Center, Tehran
Ji J, Elnashai AS, Kuchma DA (2007) An analytical framework for seismic fragility analysis of RC high-rise buildings. Eng Struct 29(12):3197–3209
Jiang H, Kurama YC (2010) Analytical modeling of medium-rise reinforced concrete shear walls. ACI Struct J 107(4):400–410
Jiang HJ, Liu LE (2011) Numerical analysis of RC shear walls under cyclic loading by Perform-3D. Adv Mater Res 250:2253–2257
Kappos AJ, Stylianidis KC, Pitilakis K (1998) Development of seismic risk scenarios based on a hybrid method of vulnerability assessment. Nat Hazards 17(2):177–192
Kim DH, Lee SG, Lee IK (2014) Seismic fragility analysis of 5 MW offshore wind turbine. Renew Energy 65:250–256
Kinali K, Ellingwood BR (2007) Seismic fragility assessment of steel frames for on sequence-based engineering: a case study for Memphis, TN. Eng Struct 29(6):1115–1127
Kircher CA, Nassar AA, Kustu O, Holmes WT (1997) Development of building damage functions for earthquake loss estimation. Earthq Spectra 13(4):663–682
Kwon OS, Elnashai AS (2006) The effect of material and ground motion uncertainty on the seismic vulnerability curves of RC structure. Eng Struct 28(2):289–303
Lignos DG, Karamanci E (2013) Drift-based and dual-parameter fragility curves for concentrically braced frames in seismic regions. J Constr Steel Res 90:209–220
Lu Y, Henry RS (2017) Numerical modelling of reinforced concrete walls with minimum vertical reinforcement. Eng Struct 143:330–345
Modica A, Stafford PJ (2014) Vector fragility surfaces for reinforced concrete frames in Europe. Bull Earthq Eng 12(4):1725–1753
Moharrami H, Amini MA (2014) Seismic vulnerability assessment of process towers using fragility curves. Struct Des Tall Spec Struct 23(8):593–603
Moravej M, Vafaei M, Abu Bakar S (2016) Seismic performance of a wall-frame air traffic control tower. Earthq Struct 10(2):463–482
Muthukumar S, Sabelli R (2013) Nonlinear seismic analysis of a round concrete tower with a post-tensioned self-centering system. In: Structures Congress 2013, 2–4 May 2013, Pittsburgh, Pennsylvania, pp 2128–2139
Mwafy A (2012) Analytically derived fragility relationships for the modern high-rise buildings in the UAE. Struct Des Tall Spec Struct 21(11):824–843
Negulescu C, Ulrich T, Bailis A, Seyedi DM (2014) Fragility curves for masonry structures submitted to permanent ground displacements and earthquakes. Nat Hazards 74(3):1461–1474
Orakcal K, Wallace JW (2006) Flexural modeling of reinforced concrete walls-experimental verification. ACI Struct J 103(2):196
Paolacci F, Giannini R (2009) Seismic reliability assessment of a disconnect switch using an effective fragility analysis. J Earthq Eng 13(2):217–235
Paolacci Fabrizio, Giannini Renato, Alessandri Silvia, De Felice Gianmarco (2014) Seismic vulnerability assessment of a high voltage disconnect switch. Soil Dyn Earthq Eng 67:198–207

Paolacci F, Phan HN, Corritore D, Alessandri S, Bursi OS, Reza MS (2015) Seismic fragility analysis of steel storage tanks. In: Proceedings of the 5th conference on computational methods in structural dynamics and earthquake engineering, 25–27 May 2015, Crete, Greece, pp 2054–2065

Porter KA, Beck JL, Shaikhutdinov RV (2002) Sensitivity of building loss estimates to major uncertain variables. Earthq Spectra 18(4):719–743

Priestley MJN (1997) Displacement-based seismic assessment of reinforced concrete buildings. J Earthq Eng 1(1):157–192

Quilligan A, O'Connor A, Pakrashi V (2012) Fragility analysis of steel and concrete wind turbine towers. Eng Struct 36:270–282

Rajeev P, Tesfamariam S (2012) Seismic fragilities of non-ductile reinforced concrete frames with consideration of soil structure interaction. Soil Dyn Earthq Eng 40:78–86

Reyes JC, Chopra AK (2011) Three-dimensional modal pushover analysis of buildings subjected to two components of ground motion, including its evaluation for tall buildings. Earthq Eng Struct Dyn 40(7):789–806

Saha SK, Sepahvand K, Matsagar VA, Jain AK, Marburg S (2013) Stochastic analysis of base-isolated liquid storage tanks with uncertain isolator parameters under random excitation. Eng Struct 57:465–474

Sarno L, Chiodi R, Manfredi G, Prota A (2013) Probabilistic assessment of seismic behaviour of an existing RC building retrofitted with BRBs. In: Proceedings of the 11th international conference on structural safety & reliability (ICOSSAR), 16–20 June 2013, New York, USA

Schotanus MI, Maffei JR (2008) Computer modeling and effective stiffness of concrete wall buildings. In: Walraven J, Stoelhorst D (eds) Tailor made concrete structures. Taylor & Francis, London, pp 939–945

SEAOC Blue Book (1999) Recommended lateral force requirements and commentary, 7th edn. Seismology Committee Structural Engineers Association of California, Sacramento

Shinozuka M, Feng MQ, Kim HK, Kim SH (2000) Nonlinear static procedure for fragility curve development. J Eng Mech 126(12):1287–1295

Siqueira GH, Sanda AS, Paultre P, Padgett JE (2014) Fragility curves for isolated bridges in eastern Canada using experimental results. Eng Struct 74:311–324

Tso WK, Zhu TJ, Heidebrecht AC (1992) Engineering implication of ground motion A/V ratio. Soil Dyn Earthq Eng 11(3):133–144

Uniform Building Code, ICBO 1997, Edition. International Conference of Building Officials, Whittier, CA

Vafaei M, Alih SC (2016) Assessment of seismic design response factors of air traffic control towers. Bull Earthq Eng 14(12):3441–3461

Vafaei M, Alih SC (2017) Seismic vulnerability of air traffic control towers. In: Lawrence D (ed) Aviation and airport security: management, improvement strategies and future challenges. Nova, New York, pp 1–20

Vafaei M, Adnan AB, Rahman ABA (2013) Seismic performance evaluation of an airport traffic control tower through linear and nonlinear analysis. Struct Infrastruct Eng 10(8):963–975

Vamvatsikos D, Cornell CA (2002) Incremental dynamic analysis. Earthq Eng Struct Dyn 31(3):491–514

Vamvatsikos D, Cornell CA (2004) Applied incremental dynamic analysis. Earthq Spectra 20(2):523–553

Wen YK, Ellingwood BR, Bracci J (2004) Vulnerability function framework for consequence-based engineering. Mid-America. Earthquake Center Project DS-4 Report. University of Illinois at Urbana-Champaign: Urbana, IL

Wilcoski J, Heymsfield E (2002) Performance and rehabilitation of type L FAA airport traffic control tower at San Carlos, California, for seismic loading. J Perform Constr Facil 16(2):85–93

Wilson JL (2003) Earthquake response of tall reinforced concrete chimneys. Eng Struct 25(1):11–24

Yang TY, Moehle JP, Bozorgnia Y, Zareian F, Wallace JW (2012) Performance assessment of tall concrete core-wall building designed using two alternative approaches. Earthq Eng Struct Dyn 41(11):1515–1531

Zhou C, Zeng X, Pan Q, Liu B (2015) Seismic fragility assessment of a tall reinforced concrete chimney. Struct Des Tall Spec Struct 24(6):440–460

Zhu TJ, Tso WK, Heidebrecht AC (1988) Effect of peak ground a/v ratio on structural damage. J Struct Eng 114(5):1019–1037